D6693 and supplemented by samples from locality 0136; neutron activation analyses of trace elements were conducted on samples from locality D6693.
12. Data from Raton Basin sites (*10*) indicate that iridium moves preferably toward organic-rich sediments, upward where peak anomalies occur near or at the base of coal seams, but downward to the same extent where the boundary clay is surrounded by coal. Officer and Drake (*3*) may have overlooked or misinterpreted these data. Their conclusion that iridium moves upward as a result of bioturbation is dubious, at least for nonmarine environments.
13. N. J. Norton and J. W. Hall, *Palaeontogr. Abt. B* **125**, 1 (1969).
14. R. Y. Anderson, *New Mexico Inst. Mines Min. Res. Mem.* **6**, 1 (1960); R. H. Tschudy, in *Cretaceous and Tertiary Rocks of the Southern Colorado Plateau*, J. E. Fassett, Ed. (Four Corners Geological Society Memoir, Farmington, NM, 1973), pp. 131–143.
15. A. R. Sweet, *Geol. Soc. Canada Econ. Rep.* 30 (1978), p. 29.
16. A. R. Sweet and L. V. Hills, in *Abstracts Sixth International Palynological Conference* (International Commission for Palynology, Calgary, 1984), abstract, p. 160.
17. J. W. Hall and N. J. Norton, *Palaeogeog. Palaeoclimatol. Palaeoecol.* **3**, 121 (1967); S. K. Srivastava, *ibid.* **7**, 221 (1970).
18. L. J. Hickey, in *Catastrophes and Earth History*, W. A. Berggren and J. A. Van Couvering, Eds. (Princeton Univ. Press, Princeton, NJ, 1984), p. 279.
19. O. B. Toon *et al.*, *Eos* **62**, 886; W. Alvarez *et al.*, *Geol. Soc. Am. Spec. Pap. 190* (1982), p. 305.
20. D. M. Jarzen, *Palynology* **2**, 29 (1978).
21. We thank R. F. Fleming and D. T. Pocknall for assistance in the field; the Los Alamos Research Reactor Group (INC-5) for neutron irradiations; R. H. Tschudy, J. A. Wolfe, D. A. Russell, and C. L. Pillmore for reviews and comments on the manuscript; and G. A. Izett who recovered the quartz grains showing shock lamellae from our samples. Two of us (C.J.O. and P.Q.O.) thank the U.S. Department of Energy for support.

3 June 1985; accepted 1 November 1985

Synthesis of Todorokite

D. C. GOLDEN, C. C. CHEN, J. B. DIXON

Todorokite of chemical composition $(Mg_{0.77}Na_{0.03})(Mg_{0.18}Mn^{2+}_{0.60}Mn^{4+}_{5.22})\ O_{12} \cdot 3.07\ H_2O$ was synthesized by a two-step procedure. First, sodium birnessite was synthesized and magnesium was exchanged for sodium to form magnesium birnessite, which was autoclaved under a saturated steam pressure at 155°C for 8 hours to form well-crystallized todorokite. Synthesized todorokite particles consisted of fibers extending from a central plate. The plate itself was made of twinned fibers forming a trilling pattern. The infrared spectra and x-ray diffraction patterns were similar to those of natural todorokite samples. Calcium birnessite and nickel birnessite, when autoclaved under conditions similar to those for magnesium birnessite, yielded a todorokite structure. However, the formation of todorokite from calcium and nickel birnessite was less extensive.

WE REPORT THE SYNTHESIS OF todorokite, which is formed principally in nature as an end product of oxidation of manganese (Mn^{2+}) in marine environments and under earth-surface conditions. There has been great interest in this tunnel-structured mineral because it is a major constituent of deep-sea manganese nodules (*1*) and has the potential of becoming a polymetallic resource of the twenty-first century (*2*). Knowing the chemistry of todorokite is important for understanding how nodules form and how they concentrate transition elements from ocean waters (*3*).

Todorokite was synthesized because natural samples of high purity are rare, and samples free of impurities and of high crystallinity are necessary for chemical and mineralogic studies. The synthesis involved a two-step procedure. First, sodium birnessite (*4*) was synthesized by oxidation of Mn^{2+} in an alkaline medium. The magnesium was then exchanged for sodium, and the magnesium birnessite was autoclaved at 155°C for 8 hours in an aqueous medium with or without excess $MgCl_2$ to obtain todorokite.

Infrared spectra of natural todorokite indicate that todorokite is not analogous to any of the synthetic phases (*5*) reported to be identical to todorokite (*6*). The largest tunnel structure reported for a synthetic manganese oxide (2 octahedra by 3 octahedra) is that of psilomelane (*7*). Tunnel-structured manganese minerals such as cryptomelane and hollandite have been synthesized by dry heating of birnessite saturated with the appropriate cations K^+ and Ba^{2+}, respectively, at 500° to 800°C (*8*). In the above syntheses, the size of the cation controls the dimensions of the tunnel (2 octahedra by 2 octahedra). However, the large size (ideally 3 octahedra by 3 octahedra) of the todorokite tunnel requires an unusually large cation. Because such an unhydrated inorganic cation does not exist, the large hydrated Mg^{2+} cation in aqueous solution was used in this preparation.

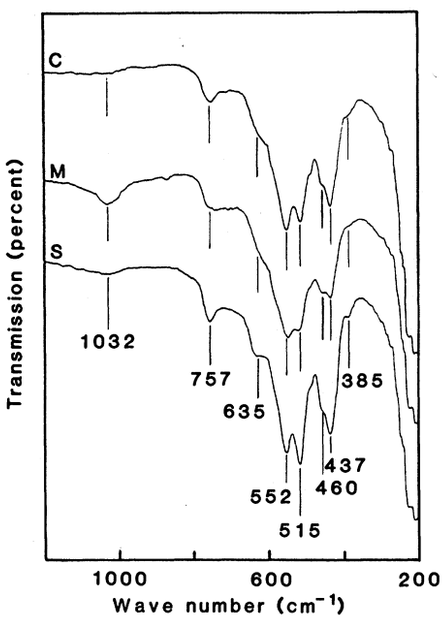

Fig. 1. Infrared spectra of synthetic todorokite (S) and natural todorokites from Montenegro mine, Cuba (M), and Charco Redondo, Cuba (C).

First, birnessite was synthesized by a modification of the procedure of Stähli (*9*). Manganese dichloride (200 ml, 0.5*M*) was placed in a 500-ml plastic beaker. Oxygen was then bubbled into the solution through a glass frit at a rate of 1.5 liters per minute [it was important to maintain this rate of oxygen flow to prevent the formation of hausmannite (Mn_3O_4)]. This was followed by the addition of 55 g of NaOH in 250 ml of H_2O.

After 5 hours oxygenation was stopped and the black precipitate (buserite) was washed with deionized water until the supernatant was salt-free. The product was freeze-dried, which dehydrated the buserite to birnessite, and stored. Infrared analysis, x-ray diffraction, and electron microscopy (*10*) indicated that birnessite was the only crystalline phase present.

In the second step, a 25-mg sample of the sodium birnessite was shaken with 20 ml of 1*N* $MgCl_2$ for 12 hours. The sample was then centrifuged and washed twice with 20-ml portions of distilled deionized water to remove the exchanged sodium. The magnesium birnessite synthesized was either dispersed in distilled water or fresh 1*N* $MgCl_2$ (20 ml). These mixtures were autoclaved at 155°C in a sealed 25-ml Teflon-lined stainless steel container under autogenous pressure for 8 hours. The container was then cooled to room temperature, and the contents were washed free of any excess $MgCl_2$ with water. The product was then freeze-dried and stored. Increased autoclaving time gives rise to slightly sharper x-ray diffraction peaks (*11*); however, it also causes the grad-

Department of Soil and Crop Sciences, Texas A&M University, College Station, 77843.

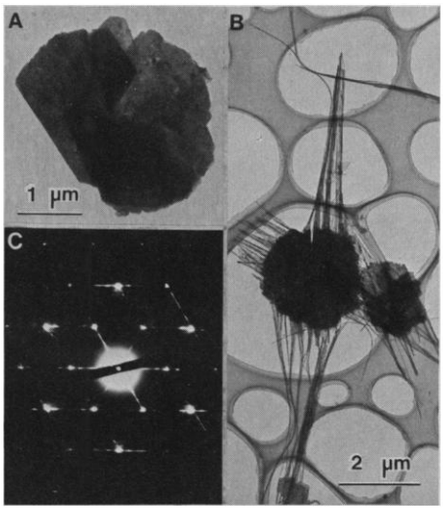

Fig. 2. Transmission electron micrograph of birnessite (A) and of synthetic todorokite, showing fibers extending from a center plate of matted fibers that retains the morphology of the parent birnessite (B). (C) Selected-area electron diffraction of the matted fibers, showing *d*-spacing randomness in three directions in the plane of view.

ual appearance of another mineral—manganite (*12*). The chemical composition of the synthetic todorokite from magnesium birnessite autoclaved for 8 hours, determined on the basis of a 12-oxygen unit cell, was $(Mg_{0.77}Na_{0.03})(Mg_{0.18}Mn^{2+}_{0.60}Mn^{4+}_{5.22})O_{12} \cdot 3.07$ H_2O (*13*).

The synthetic samples were analyzed by x-ray diffraction, with a quartz internal standard (4 percent by weight) used for positioning the diffraction peaks. The x-ray powder diffraction data for the synthetic sample and for todorokite (*14*) were in good agreement (Table 1).

The infrared spectrum (Fig. 1) of synthetic todorokite (S) matches well with those of the natural todorokite samples from Charco Redondo, Cuba (C). The natural todorokite sample (M) from Montenegro mine, Cuba (USNM 113966), has an additional band at 1032 cm^{-1} due to a silicate contaminant. The todorokite sample from Charo Redondo was free of contaminants. Todorokite spectra are distinct from those of birnessite (*5*). The bands are sharper and more intense for the synthetic todorokite sample than those for natural samples. According to Potter and Rossman (*5*), the infrared spectrum can unambiguously distinguish well-crystallized todorokite from other manganese minerals. The infrared patterns indicate that our synthetic sample is similar in crystallinity to the well-crystallized natural sample from Charco Redondo (*5*). Infrared spectra for natural todorokites show changes in relative intensity of bands even among pure specimens (*15*).

The morphology of the synthetic todorokite consists of fibers extending from a central plate (Fig. 2B), which retained a shape similar to that of the parent birnessite (Fig. 2A). The electron diffraction pattern (Fig. 2C) of the plate has pseudohexagonal symmetry resulting from the fibers running in three directions (Fig. 3A). These fibers are 20 to 50 nm in width and 50 μm or less in length. They are morphologically similar to those of the natural todorokite sample from Montenegro mine and to those of samples described by other investigators (*7, 16*). The fibers were fragile and easily broken into shorter sections upon sonication.

The trilling pattern (Fig. 3A) of the twinned crystals is typical of todorokite (*3, 17*) and distinguishes it from the platy birnessite parent compound. The lattice fringes obtained by high-resolution transmission electron microscopy (HRTEM) (Fig. 3B) show a common *a* dimension of about 1 nm, which indicates a tunnel width in one direction of 3 octahedra. This spacing is in accordance with that found by Straczek and colleagues (*18*), who reported an orthorhombic or a monoclinic unit cell of $a = 0.975$ nm, $b = 0.284$ nm, $c = 0.959$ nm, and $\beta \simeq 90°$ for todorokite. A structural model of 3 by 3 tunnel dimensions for todorokite, based on HRTEM observations

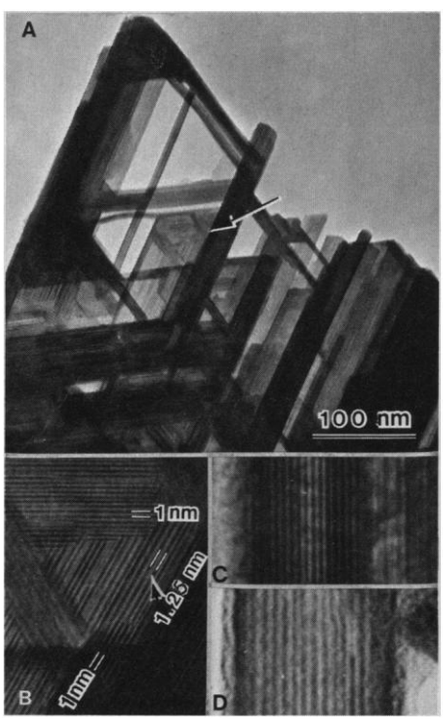

Fig. 3. (A) High-resolution transmission electron micrograph of synthetic todorokite, showing the trilling pattern of the matted fibers. (B) Enlarged view of area indicated by the arrow in (A). (C) An individual fiber showing uniform 1-nm spacings in the *a* direction. (D) An individual fiber, showing mainly 1.25-nm spacings in the *a* direction.

Table 1. X-ray powder diffraction data for synthetic and natural todorokite. *I*, relative band intensity.

Synthetic todorokite		Natural todorokite*	
d-spacing (nm)	*I* (%)	*d*-spacing (nm)	*I* (%)
0.966	100	0.968	100
0.713	5	0.715	2
0.480	80	0.480	80
0.444	10	0.445	5
0.320	5	0.322	15
0.248	20	0.246	20
0.239	20	0.239	40
0.234	10	0.234	15
0.223	10	0.222	20
0.215	4	0.215	5
0.197	5	0.198	20
0.195	5	0.192	5
0.175	10	0.175	10
0.154	5	0.154	5

*Todorokite from Todoroki mine, Japan (*14*).

of thin sections of natural todorokite, has been proposed (*3, 19*). The heterogeneity in the channel sizes typical of natural todorokites (*13, 17*) was also apparent in the synthetic sample (Fig. 3, B, C, and D). Spacings of 1, 1.25, 1.5, and 2 nm were observed for the *a* parameter in three directions parallel to the plate. However, 0.96 nm was the predominant *d*-spacing, as suggested by the sharp x-ray diffraction peaks of the oriented sample in the direction perpendicular to the plate (*c*). Therefore, our synthesis procedure produced a material similar to natural todorokite with predominant tunnel sizes of 3 octahedra by 3 octahedra.

Calcium, nickel, and cobalt were also used as saturating cations in the synthesis procedure. Autoclaved calcium birnessite and todorokite have similar x-ray diffraction patterns and infrared spectra; however, broad infrared and diffraction bands indicated disorder in the crystals. Channel dimensions for autoclaved calcium birnessite in the *a* direction as observed by HRTEM were 0.75, 1.0, and 1.25 nm. A nickel-saturated sample yielded two phases as identified by HRTEM: a todorokite-like phase with predominantly 0.5- and 1-nm *a* dimensions, and another phase consisting of electron-dense hexagonal plates in minor quantities. In the case of autoclaved cobalt birnessite, no tunnels were detected by HRTEM. Magnesium birnessite, upon autoclaving, yielded the best crystallized todorokite.

REFERENCES AND NOTES

1. R. G. Burns and V. M. Burns, in *Marine Minerals*, R. G. Burns, Ed. (LithoCrafters, Chelsea, MI, 1979), pp. 1–46; in *Marine Manganese Deposits*, G. P. Glasby, Ed. (Elsevier, Amsterdam, 1977), pp. 185–1248; *Philos. Trans. R. Soc. London* **285**, 249 (1977).
2. ———, *Philos. Trans. R. Soc. London* **286**, 283 (1977); ———, H. W. Stockman, *Am. Mineral.* **70**, 205 (1985).

3. S. Turner and P. R. Buseck, *Science* **212**, 1024 (1981).
4. Magnesium- or sodium-saturated birnessite in aqueous medium or high relative humidity expands to approximately 1-nm basal spacing (buserite); however, for simplicity we use the term birnessite throughout this report.
5. R. M. Potter and G. R. Rossman, *Am. Mineral.* **64**, 1199 (1979).
6. R. M. McKenzie, *Mineral. Mag.* **38**, 294 (1971); R. Giovanoli and P. Bürki, *Chimia* **29**, 114 (1975).
7. R. G. Burns, V. M. Burns, H. W. Stockman, *Am. Mineral.* **68**, 972 (1983); R. Giovanoli, *ibid.* **70**, 202 (1985).
8. R. Giovanoli and B. Balmer, *Chimia* **35**, 53 (1981).
9. E. Stähli, thesis, University of Berne, Switzerland (1968).
10. Infrared spectroscopy of todorokite was performed by making pellets with anhydrous KBr (0.3 mg of todorokite per 300 mg of KBr) at a pressure of 1.38×10^5 kPa for 5 minutes. Bands in the range of 200 to 250 cm^{-1} were not considered because of the overlap of the KBr absorption. HRTEM was performed on todorokite suspensions dried on a holey carbon grid with a Zeiss 10C electron microscope operated at 60 or 100 kV. A Philips Norelco x-ray diffractometer equipped with a graphite monochromator was used for x-ray diffraction of random powder mounts of todorokite using CuKα radiation.
11. A statistical analysis using the t statistic of the mean channel dimensions of samples (1.11 nm) autoclaved for 48 hours versus samples (1.08 nm) autoclaved for 8 hours showed no significant difference ($t = 0.7146$, d.f. = 38; $P > 0.48$).
12. Manganite crystals were large and separated from the todorokite crystals, when viewed by TEM, and showed no evidence of topotactic transformation from birnessite or todorokite.
13. Chemical analysis of todorokite and determination of the oxidation state of manganese was done by the method of J. D. Hem [*Geochim. Cosmochim. Acta* **45**, 1369 (1981)]. In assigning the cations, a 12-oxygen unit cell was assumed. Although the presence of Mn^{3+} in the structure of todorokite has been demonstrated, in this study atomic assignments were done by assuming the presence of only two species, Mn^{2+} and Mn^{4+}. Sodium was considered a tunnel cation, whereas magnesium was considered both a tunnel and a structural cation. No chloride or silicon were detected in synthetic todorokite.
14. C. Frondel, U. B. Marvin, J. Ito, *Am. Mineral.* **45**, 1167 (1960).
15. Samples show changes in intensities of bands between 400 and 600 cm^{-1}. The variation of intensities in our synthetic samples falls within this range. See Fig. 16, samples 58 and 60, in (5).
16. R. Giovanoli, in *Geology and Geochemistry of Manganese*, I. M. Varentsov and G. Grasselly, Eds. (Akedemiai Kiado, Budapest, 1980), pp. 160–202.
17. F. V. Chukhrov, A. I. Gorshkov, A. V. Sivtsov, V. V. Beresovskaya, *Nature (London)* **278**, 631 (1979).
18. J. A. Straczek, A. Horen, M. Ross, C. M. Warshaw. *Am. Mineral.* **45**, 1174 (1960).
19. S. Turner, M. D. Siegel, P. R. Buseck, *Nature (London)* **296**, 841 (1982).
20. We thank R. Giovanoli for generously sharing his publications; G. Rossman for sending the reference samples of todorokite; the Electron Microscopy Center, Texas A&M University, for providing facilities for TEM; and N. Lee for technical assistance.

30 July 1985; accepted 18 November 1985

E1A Transcription Induction: Enhanced Binding of a Factor to Upstream Promoter Sequences

IMRE KOVESDI, RONALD REICHEL, JOSEPH R. NEVINS

The adenovirus E1A gene product *trans*-activates a number of viral and cellular promoters. The mechanism for this transcriptional induction was investigated with an in vivo exoIII mapping technique to assay for proteins that interact with an E1A-inducible promoter. A protein bound to the early E2 promoter was detected in wild-type infected cells. In the absence of E1A induction, specific interactions at the promoter could not be detected, as indicated by the absence of an exoIII-protected fragment. However, if conditions were established that allowed transcription of the E2 gene in the absence of E1A, the same exoIII protection was observed as was found in the presence of E1A. These results suggest a model in which the efficient utilization of the E2 promoter is mediated by a cellular transcription factor. In the absence of E1A, the interaction can take place, but slowly and inefficiently in comparison with the interaction in the presence of E1A.

THE PROCESS BY WHICH THE INITIATION of transcription is regulated, while of central importance to many aspects of biology, is not clearly understood. The critical aspects of the process are the protein factors that interact with regulatory sites of promoters and the manner in which the activity of these factors is controlled. A particularly useful system for the study of transcriptional control are the early genes of adenovirus. The regulatory gene that is responsible for this control, the E1A gene, has been identified (*1–3*). A set of five viral promoters are coordinately regulated. In addition, two cellular promoters, hsp70 and β-tubulin, are stimulated by the action of the E1A gene product (*4–6*). Therefore, all of the components of a system of transcriptional control are contained within an early viral infection: genes that respond to positive control, an identified regulatory gene, a set of coordinately controlled genes, and genes in a distinct context (cellular chromosome) that are coordinately controlled.

To gain further insight into the mechanism of E1A-mediated transcription control, we analyzed adenovirus chromatin in infected cells for the presence of proteins in the vicinity of a promoter controlled by E1A—in this case the E2 promoter. We and others have shown that this promoter is inducible by E1A and requires certain upstream sequences for activity (*7–12*). The fact that there exist sequences critical for promoter activity suggests that a protein or proteins may recognize these sequences. To identify such interactions, we used a technique, described by Wu (*13*), in which exonuclease III (exoIII) defines protein-DNA interactions in vivo. The rationale for the procedure in the context of the adenovirus E2 promoter is shown schematically in Fig. 1A. Briefly, nuclei are incubated with a restriction endonuclease for which there is a recognition site in the vicinity of the suspected protein binding site. In the case of the E2 promoter, there is an Eco RI site at −285 relative to the transcription initiation site (+1). Therefore, nuclei are incubated with Eco RI in the presence or absence of exoIII. The DNA is extracted and purified and subsequently digested with S1 nuclease to remove the single-strand tail resulting from exoIII digestion and then digested with a second restriction enzyme, in this case Sst I. The digested DNA is then separated in an agarose gel, transferred to nitrocellulose, and visualized with a probe specific to the sequence adjacent to the Sst I site. Three possible DNA fragments can be detected in this way. An Sst I–Sst I band would be present if the Eco RI digestion was not complete. An Sst I–Eco RI fragment is produced in the absence of exoIII digestion. Finally, if a protein is stably bound in a nonrandom fashion to a specific site on the DNA, then exoIII digestion is stopped and a band is produced that is smaller than the Sst I–Eco RI fragment.

Such an analysis was performed with nuclei from cells infected with wild-type adenovirus 5 (Ad5) for 7 hours, in the presence of arabinosylcytosine to prevent DNA replication (Fig. 1B). In the absence of exoIII, two bands are detected and represent the Sst I–Sst I fragment and the Sst I–Eco RI fragment. In this experiment and most others that have been done, approximately 50 percent of the adenovirus chromatin is cut by Eco RI. As the amount of exoIII added to the nuclei is increased, there is the appearance of lower molecular weight bands. At the highest exoIII concentration, a band of 995 nucleotides predominates. Such a fragment indicates that the exoIII stop is at a position of −85 relative to the E2 transcription initiation site (Fig. 1C). There are intermediate-sized bands, apparently the result of incomplete exoIII digestion since they tend to disappear at higher enzyme

The Rockefeller University, New York, NY 10021